

SHEAR COAXIAL INJECTOR ATOMIZATION PHENOMENA FOR
COMBUSTING AND NON-COMBUSTING CONDITIONS

S. Pal*, M. D. Moser†, H. M. Ryan†, M. J. Foust† and R. J. Santoro‡

Propulsion Engineering Research Center

and

Department of Mechanical Engineering

The Pennsylvania State University

University Park, PA 16802-2320

GRANT
IN-34-CR
180877
p. 39

-
- * Research Associate, Mechanical Engineering
 - † Graduate Student, Mechanical Engineering
 - ‡ Professor, Mechanical Engineering

(NASA-CR-193339) SHEAR COAXIAL
INJECTOR ATOMIZATION PHENOMENA FOR
COMBUSTING AND NON-COMBUSTING
CONDITIONS (Pennsylvania State
Univ.) 39 p

N94-11526

Unclas

G3/34 0180877

ABSTRACT

Measurements of LOX drop size and velocity in a uni-element liquid propellant rocket chamber are presented. The use of the Phase Doppler Particle Analyzer in obtaining temporally-averaged probability density functions of drop size in a harsh rocket environment has been demonstrated. Complementary measurements of drop size/velocity for simulants under cold flow conditions are also presented. The drop size/velocity measurements made for combusting and cold flow conditions are compared, and the results indicate that there are significant differences in the two flowfields.

INTRODUCTION

The steady state combustion process in a bi-propellant liquid rocket engine includes liquid propellant injection, atomization, vaporization, mixing with its counterpart propellant which is either injected in gas phase or is vaporized in a similar manner, and finally, combustion. Clearly, the process starts with the injection and subsequent atomization of the liquid propellant, and this mechanism in turn defines the flowfield and combustion characteristics in the rocket chamber. The fluid injection and atomization process involves the use of a manifold of injectors, with the type of injector usually dictated by propellant type and combustion stability considerations. Historically, for the liquid oxygen (LOX)/gaseous hydrogen (GH_2) propellant combination, the element of choice has been the shear coaxial injector, although recently the swirl coaxial injector has been proposed as an alternative/advancement because of its 'self-atomization' characteristics. The shear coaxial injector has been successfully used in the J-2, RL10A-1 and Space Shuttle Main Engine (SSME) [1] and the swirl coaxial injector has been used in the RL10A-3 [1] and is also proposed for use in the Space Transportation Main Engine

(STME) [2]. For liquid/liquid propellant combinations like RP-1/LOX or storables like nitrogen tetroxide(NTO)/monomethyl hydrazine (MMH), the element of choice has been the impinging injector. Engines which have used impinging injectors include the F-1, H-1, Titan and XLR-132 [1].

Understanding the physics of the atomization process for a particular injector is critical for understanding the subsequent dynamics of vaporization, mixing and combustion. This level of understanding can only be obtained by experiments that detail both the evolving drop size/velocity fields and the gas phase velocity field under combusting conditions, and theoretical models based on first principles that corroborate the measurements. Currently, the data base for drop size/velocity fields under combusting conditions is minimal and consequently, atomization models for predicting initial drop size distributions that are incorporated in computational fluid dynamics (CFD) codes for predicting the steady state combustion phenomena are either based on analytical treatments such as linear stability theory or extrapolations of parametric correlations of drop size obtained for cold flow conditions [3-5]. A data base of drop size distribution data for combusting conditions is therefore critical for verifying/refuting both atomization models and the practice of extrapolating drop size correlations obtained for cold flow conditions to predict drop size for combusting conditions. It is important to realize that the physical parameter space in terms of pressure, temperature, Reynolds number and Weber number for typical cold flow experiments is significantly different from that found for combusting conditions. Finally, a drop size distribution data base for combusting conditions could be used for developing correlations that are directly input into CFD codes.

The number of experiments designed in the past to address this void in drop size data for combusting conditions is minimal because of the general lack of diagnostic techniques capable of probing the harsh environment in a liquid propellant rocket chamber, the safety aspects that have to be strictly adhered to in handling propellants that range from hypergolic to cryogenic fluids and the expensive nature of these experiments. To the authors' knowledge, the experiments reported by George [6-7] is the only program that has attempted to address the need for drop size data under combusting conditions. George measured drop sizes from holographic images of the spray formed from a uni-element like-on-like impinging doublet injector in a transparent side-walled thrust chamber. The propellant combination was gaseous N_2O_4 oxidizer injected through holes on the face plate and liquid N_2H_4 fuel injected through a doublet injector to form the drop cloud. George [6-7] also conducted complementary cold-flow experiments using water and nitrogen as simulants and his comparisons of the two sets of drop size measurements showed significant differences between the measured drop sizes, thus indicating the need for additional hot-fire experiments to characterize actual rocket sprays.

In the last decade, phase Doppler interferometry [8-9] has advanced to a stage where temporally-averaged drop size distributions as a function of spatial position can be obtained in harsh environments. Researchers have used this technique for measuring drop size and velocity in sprays ranging from oil burner to diesel applications [10]. This technique has also been used to characterize the drop field in sprays formed by rocket injectors for cold flow conditions, where simulants are used instead of actual propellants (for example, Refs. 11-14). In addition, Goix et al. [15] have recently used this technique for measuring drop size in a methanol/air flame from a coaxial injector.

The present effort is geared towards systematically mapping the drop size field downstream of a shear coaxial injector in a rocket chamber that combusts gaseous hydrogen with liquid oxygen. Measurements of LOX drop size under combusting conditions made using the phase Doppler particle interferometry technique are presented and compared with complementary drop size measurements made under cold flow conditions with water and gaseous nitrogen (GN_2) as simulants.

EXPERIMENTAL

The experiments were conducted at the Cryogenic Combustion Laboratory located at Penn State University. This laboratory provides the capability for firing both gaseous and liquid propellant sub-scale rockets. The flowrate capabilities of this laboratory are 0.45 kg/s for liquid oxygen (LOX) and 0.11 kg/s for gaseous hydrogen (GH_2).

Hot-Fire Studies

The rocket chamber used for these experiments is modular in design and provides optical access for laser-based diagnostic approaches. A cross-sectional view of the chamber is shown in Fig. 1. The chamber consists of an injector assembly section, a window-section, an igniter section, several blank sections and a nozzle section, which are held in place by a hydraulic jack. The middle sections of the chamber can be interchanged, allowing placement of the window-section at any location along the chamber. This arrangement provides optical access along the entire length of the chamber, while also allowing the chamber length to be varied by removing or installing blank sections. For the experiments reported here, the length of the chamber was 245.6 mm. The window section includes two diametrically opposed quartz windows, 50.8 mm in diameter that provide optical access to the 50.8 mm square cross-section combustion chamber.

The other two sides of this section feature slot windows measuring 6.25 x 50.8 mm which provide additional optical access. All of the windows are thermally protected from the hot combustion gases by a curtain purge of nitrogen which flows across the windows. The injector section also has a modular design that allows for easy change of injector type and/or geometry. For these experiments, the element was a shear coaxial injector as shown in Fig. 2. The inner diameter of the LOX post (d) was 3.43 mm and the post was recessed 3.78 mm. The inner diameter of the fuel annulus was 4.19 mm and the outer diameter was 7.11 mm. The dimensions of this injector are comparable to the fuel and oxidizer pre-burner elements of the Space Shuttle Main Engine (SSME).

The igniter section of the rocket chamber is equipped with an ignition chamber (not shown in Fig. 1) that provides a spark-ignited gaseous hydrogen/gaseous oxygen torch for ignition in the main combustion chamber. Finally, the water-cooled nozzle of the rocket can be easily changed to vary the chamber pressure. For the present experiment, the nozzle had a throat diameter of 11.36 mm. These design features allow the study of the combustion inside the rocket over a wide range of injector geometries and operating conditions.

The setting/monitoring of the flowrate of the gaseous (GH_2) and liquid (LOX) propellants was accomplished with the aid of a critical orifice and a cavitating venturi, respectively, that were instrumented at both upstream and downstream locations with pressure transducers and thermocouples. The nominal LOX and GH_2 flowrates were 0.113 kg/s and 0.022 kg/s respectively, thus resulting in an O/F mass flow ratio of 5.1:1. These flowrates, coupled with the nozzle dimensions yielded a chamber pressure of 2.74 MPa (\approx 400 psia).

The duration of a test run was four seconds and represents a compromise between the time required to achieve steady-state chamber pressure and quartz window survivability. For these tests, it takes in excess of two seconds for the chamber pressure to stabilize. The cause of this rough startup transient has yet to be identified. However, following this two second transient period, the chamber pressure remains steady for the duration of the test.

The LOX flowfield was first visually characterized using a laser sheet technique. These experiments provided preliminary information on the fluid dynamics of the LOX core breakup process and also helped in guiding the approach for measuring LOX drop size and velocity using phase Doppler interferometry. A laser sheet formed from the continuous wave beam of an argon-ion laser (514.5 nm) was introduced through one of the slot windows. A video camera equipped with a 10 nm bandpass filter centered around 514.5 nm was used to record the scattered light from the LOX flowfield through one of the circular windows. The bandpass filter was used to reject light from the luminous flame. The video images indicated that the LOX jet seemed intact for about 50 mm from the injector face. Downstream of this location, the images indicated the possible presence of a drop field. These initial experiments provided a qualitative picture of the disintegrating LOX jet and indicated the locations within the flame front where LOX drop size measurements should be attempted.

The Phase Doppler Particle Analyzer (PDPA) is a commercially available instrument capable of measuring liquid drop size and velocity based on phase Doppler interferometric theory [8-9]. The PDPA instrument was used to measure LOX drop size and velocity in the above described rocket chamber under combusting conditions. The PDPA is a point measurement technique that has been used extensively over the last decade by several researchers

(for example, Refs. 8-16). The PDPA instrument extends the basic principles of the conventional dual beam laser Doppler velocimeter to obtain particle size in addition to velocity. An argon-ion laser beam is split into two equal intensity beams and focused to an intersection to form a probe volume as shown in Fig. 3. For the present experiment, the receiver system was located at a 30° off axis angle to best exploit the characteristics of the interference pattern of the refractive LOX drops. This was achieved by inclining both the transmitting and receiving optics at a 15° angle, thus resulting in a net 30° off-axis angle. A 10 nm bandpass filter centered around 514.5 nm was placed in front of the collection optics to reject light from the luminous flame. Note that the collection optics of the receiving system coupled with the transmitting optics define the probe volume characteristics. In addition to the collection optics, the receiving system consists of three detectors at appropriate separations that independently measure the burst signal generated by drops traversing the probe volume, albeit with a phase shift. The velocity of the particle is then extracted from the temporal frequency of the burst signal, whereas the particle size is calculated from the measured phase shift between any two detectors and the *a priori* calculated linearity between the detector separation and the phase angle. The index of refraction of the liquid drop being measured enters into this analysis, and is 1.221 for LOX [17].

Cold Flow Studies

A sequence of cold flow drop size measurement experiments were also carried out to form a basis for comparison with the drop sizes measured for the hot-fire experiments. The design of the cold flow experiments considered both geometrical and flow parameter similitude. In terms of the geometry, the injector used for the hot-fire experiments was also

used for the cold flow experiments. To maintain exact flow parameter similitude between the two sets of experiments, the propellants used for the hot-fire, i.e. LOX and GH_2 , would have to be used at the elevated chamber pressure (≈ 2.74 MPa). This experiment is possible and requires a nozzle with an extremely small throat to achieve the elevated pressure. However, the obvious hazards associated with this experiment suggested that simulants would have to be used for the cold flow experiments, thus compromising exact flow parameter matching. The cold flow experiments were conducted at atmospheric pressure with water and gaseous nitrogen (GN_2) as simulants for LOX and GH_2 . The physical properties of the propellants are compared with those of the simulants in Table 1. The density of water is comparable to that of LOX, but the viscosities and surface tension are significantly different. Consequently, for same flowrates and geometries, the Reynolds and Weber numbers for the hot-fire experiments are an order of magnitude greater than for the cold flow experiments. This point will be revisited in a later section. At atmospheric pressure, GN_2 is 14 times more dense than GH_2 , but since the hot-fire experiments were for an elevated pressure (≈ 2.74 MPa), the density difference between the two gases is less than a factor of two when comparing the two at the actual chamber conditions.

The PDPA instrument was used to measure water drop size and velocity for the spray emanating from the same injector used for the hot-fire experiments. For these atmospheric pressure experiments, to accommodate water collection, the spray was made to develop in the downward direction. Therefore, the orientation of the PDPA instrument was changed accordingly (same 30° off-axis collection but in a different plane than shown in Fig. 3). The value of 1.33 for the index of refraction of water [17] was input into the PDPA analysis.

The drop size measurements for the cold flow experiments were for three different flowrate combinations as shown in Table 2. For all three combinations, the GN_2 flowrate was set at 0.009 kg/s. The mean exit velocity from the annulus of the injector corresponding to this flowrate is 293 m/s. Higher gas flowrates were not considered so as not to choke the flow (speed of sound in nitrogen is 353 m/s). Three different water flowrates were used, viz. 0.026, 0.13 and 0.26 kg/s. Note that the three chosen flowrates envelop the LOX flowrate used for the hot-fire experiments.

RESULTS AND DISCUSSION

Hot-Fire Measurements

The PDPA instrument was used to measure LOX drops at two axial locations downstream of the injector, 38 mm and 63.5 mm. In terms of LOX post inner diameter, d , these axial locations correspond to Z/d of 11.1 and 18.5. At the 11.1 Z/d location, only about ten drops were measured over a four second run. The lack of any significant number of drop measurements at this location agrees with the video images of scattered light which showed the presence of a solid fluid structure that could be interpreted as either an intact liquid core or an impenetrable dense drop cloud. Further downstream ($Z/d=18.5$), LOX drops were measured at different radial distances from the centerline. The drop measurements are tabulated in Table 3 and the corresponding operating parameters of the rocket and shear coaxial injector in Table 4. The results are for four equally spaced radial locations, extending up to 9.5 mm from the centerline. Again, in terms of LOX post inner diameter, d , this corresponds to R/d of 2.8. At radial locations greater than R/d of 2.8, no drops were measured indicating that the drop field is confined to a narrow circumferential region. As mentioned before, the chamber pressure

traces indicated a startup transient during a four second test run. The drop size measurements are therefore shown for both the entire four second run and the time duration of steady chamber pressure. Table 3 shows the total number of measured drops along with the arithmetic mean diameter (D_{10}), Sauter mean diameter (D_{32}), mean drop velocity (U_D) and percent validation. The percent validation number represents the percentage of drops that was accepted by the instrument as being spherical drops. The PDPA instrument rejects measurements based on drop asphericity, signal to noise limits and both velocity and size dynamic range limits.

Both D_{10} and D_{32} decrease with radial distance for the steady chamber pressure period. Note that the chosen optical configuration corresponds to a size measurement range between 4-164 μm . There could possibly be a few drops greater than 164 μm , which, if measured, would increase D_{10} and D_{32} . The number of total drops measured during a four second test run decreased with radial distance indicating a decrease in the number density of drops. Inspection of the number of measured drops and percent validation during the steady chamber pressure duration shows that the values at the centerline are low compared to the other radial locations. These low values are probably a result of dense drop number densities at the centerline which lead to a large number of signal to noise errors. The corresponding operating conditions of the rocket (Table 4) show that the chamber pressure, LOX and GH_2 flowrates are repeatable for different test runs. The Reynolds number of the LOX jet is about 5×10^5 and indicates that the jet is turbulent. The mean velocity of the LOX jet is 13.5 m/s and the velocity ratio between LOX jet and annular GH_2 flow ranges from 26 to 29 between different test runs. Comparison of the LOX jet velocity with the mean drop velocity indicates that the drops are accelerating slightly as they are entrained in the higher velocity coaxial gas stream. Finally, the high

operating Reynolds and Weber numbers are comparable to those encountered in actual liquid propellant rockets.

The probability density function of LOX drops measured for Run 2 (Table 3) is shown in Fig. 4. The probability density function of drop size for both the entire four second test and for the steady chamber pressure time interval (1.03 sec.) are depicted in this figure. The probability density functions are mono-modal, peak between 20 to 30 μm , and are positively skewed. It is evident from the figure that the probability density function of drop size for the steady-state chamber pressure interval is "noisy" compared to that for the entire test run and stems from the order of magnitude difference in sample size. Furthermore, the probability density function for the steady-state time interval has larger moment diameters (D_{10} , D_{32} , etc.) and indicates that the atomization phenomenon during the transient chamber pressure startup time interval is different from that during the steady state chamber pressure interval. Probability density functions for the other test runs show the same trends.

Cold Flow Measurements

Drop size and velocity measurements were made in the water/ GN_2 coaxial injector sprays with the PDPA instrument. The measurements for all three parametric conditions (see Table 2) were made at one axial location, 50.8 mm ($Z/d=14.8$) downstream of the injector face. At the axial location, drop size/velocity measurements were made at 3.18 mm intervals in the radial direction. For some cases, measurements at finer radial intervals (1.59 mm) were also made. A typical data set for the calculation of the various mean diameters included in excess of 8000 drop size/velocity measurements.

The measured Sauter mean diameter (D_{32}) is plotted versus nondimensionalized radial distance, R/d , for the three flow conditions in Fig. 5. For all three flow conditions, the mean exit gas velocity from the annulus of the injector is 293 m/s, whereas the liquid velocities are 2.9, 14.3 and 28.3 m/s, respectively. Comparisons between these measurements therefore highlight the effects of liquid flowrate on drop size. For each flow condition, D_{32} is maximum at the centerline, decreases with radial distance to a minimum and finally increases slightly near the edge of the spray. Both Zaller [12] and Eroglu and Chigier [13] observed similar trends in PDPA measurements of drop size in coaxial injector sprays. Hardalupas et al. [14] also reported drop size measurements with similar trends at an axial location close to the injector. However, their measurements at greater axial locations did not show the slight increase in drop size at the edge of the spray. From the measurements shown in Fig. 5, it is evident that near the central part of the spray, the mean drop size, D_{32} , increases with increasing water flowrate (or decreasing gas to liquid momentum ratio), indicating poorer atomization. However, near the edge of the spray, $R/d > 5$, D_{32} for all three flow conditions approaches the same value.

The complementary mean drop velocity, U_D , is plotted in a similar manner in Fig. 6. For a given flow combination, the mean drop velocity increases to a maximum with radial distance from the centerline and then decreases for greater radial distances. The value of the maximum mean drop velocity is significantly lower than the mean exit gas velocity suggesting that the gas phase velocity has decelerated considerably at this axial location. Near the centerline, the bigger mean drops corresponding to the higher liquid flowrates have a lower mean velocity because the larger drops respond more slowly to the gas flow than smaller drops.

As mentioned before, the PDPA instrument rejects measurements based on drop asphericity, signal to noise limits and both velocity and size dynamic range limits. The corresponding percent validation and samples per second for the drop size/velocity measurements are depicted in Figs. 7 and 8. For the two lower liquid velocity cases, the percent validation at all radial measurement locations ranges between 80 to 90%. These high validation percentages for PDPA measurements are characteristic of locations within sprays where drops are spherical and the signal to noise ratio is high. However, for the highest liquid velocity case, the percent validation is low at and near the centerline, indicating that the liquid jet has not completely atomized into spherical drops. Additional insight on the spray development characteristics can be gained by perusing the measured samples per second versus radial location plot, Fig. 8. For all three velocity cases, the measured samples per second is low at the centerline, increases with radial distance to a maximum and then decreases for greater radial distances. For the lowest velocity case, the measured samples per second at the centerline is significant ($> 1500/s$), whereas for the two highest velocity cases, it is near zero. The percent validation and samples per second results indicate that for the lowest liquid velocity case, the spray at the axial measurement location is atomized completely, i.e. all the drops are spherical. For the two highest liquid velocity cases, the low number of samples per second at the centerline suggest that the spray is not completely atomized, i.e. the liquid jet could be intact or there could be large ligament structures present.

Hot-Fire/Cold Flow Comparisons

The cold flow and hot-fire experiments were identical in terms of geometry but differed in terms of flow parameters. However, in terms of both liquid and gas flowrates, the hot-fire

experiment was comparable to the second cold flow experiment (Table 2, case 2). Therefore, a comparison of the drop size/velocity measurements for these two cases provides some insight on the general differences between hot-fire and cold flow experiments.

A comparison of the flow parameters for both the hot-fire and cold flow (Table 2, case 2) experiments is presented in Table 5. The flow parameters listed are the chamber pressure, mass flowrates and velocities for both the liquid and the gas, the mass flowrate, velocity and momentum ratios between the gas and the liquid, the Reynolds number of the liquid jet, and the Weber number. The hot-fire to cold flow parametric ratios are also presented in the table. For example, the ambient pressure, P_c , was 2.67 MPa for the hot-fire experiment and 0.1 MPa for the cold flow experiment, yielding a ratio of 26.3. In comparing the parameters for the two experiments, it is readily discerned that with the exception of the chamber pressure, Reynolds number and Weber number, all the other parameters are within the same order of magnitude. The chamber pressure is not of primary importance because its only contribution to the atomization phenomenon is to affect the gas density. Therefore, in comparing the two experiments, the only parameters that differ by greater than an order of magnitude are the Reynolds and Weber numbers. These two parameters differ because LOX and water have different dynamic viscosities and surface tensions (see Table 1).

Keeping in mind the aforementioned differences, the radial variations of measured Sauter mean diameter, D_{32} , and mean drop velocity, U_D , for both the hot-fire and cold flow cases are compared in Figs. 9 and 10, respectively. The D_{32} measurements compared in Fig. 9 show that the drop cloud extends further in the radial direction for the cold flow case. This observation makes intuitive sense because LOX drops vaporize and combust whereas water drops do not

evaporate. The measured drop size for the hot-fire case is also larger than for the cold flow case. At first glance, the differences in flow conditions between the two experiments (Table 5) makes any comparison between the two sprays seem futile. However, a thought experiment is helpful here. If one envisions a cold flow experiment with the same water and GN_2 velocities, but at an elevated chamber pressure of 0.23 MPa, then except for the Reynolds and Weber numbers, all the flow parameter ratios listed in Table 5 would be very close to one. The mean drop size for such an experiment would be smaller than the measured drop size for the cold flow experiment shown in Fig. 9, because the higher gas mass flowrate and momentum would atomize the liquid jet more effectively. The measurements therefore indicate that the mean drop size for a hot-fire experiment is larger than for a cold flow experiment, with all flow parameters being equal except for the Reynolds and Weber numbers which are higher for the hot-fire case. This observation is counter intuitive and suggests that there are significant differences in the atomization process between cold flow and hot-fire conditions. The gas phase velocity field in a combusting flow is probably radically different from the cold flow case thus altering the shear mechanism that is responsible for atomization.

The radial variation of mean drop velocity for the hot-fire experiment is compared to that for the cold flow case in Fig. 10. Here, the mean drop velocity for the cold flow case is greater than that for the hot-fire case. The larger drops present in the hot-fire case would be expected to accelerate slower than the smaller drops present in the cold flow case. Additionally, a slower gas phase velocity field for the hot-fire case would produce larger drops and also retard the acceleration of the drops.

SUMMARY

Drop size and velocity were measured with a Phase Doppler Particle Analyzer (PDPA) instrument in a uni-element (shear coaxial injector) rocket chamber under combusting conditions for the liquid oxygen (LOX)/gaseous hydrogen (GH_2) propellant combination. Complementary PDPA drop size/velocity measurements were also made in the spray from the same injector with water and gaseous nitrogen (GN_2) simulating LOX/ GH_2 . The flow conditions of the cold flow experiments were similar to the hot-fire experiments in terms of both flowrates and velocities for both the liquid and the gas, but differed by an order of magnitude in terms of Reynolds and Weber numbers as depicted in Fig. 11. The hot-fire experiment is similar to actual rocket conditions in terms of these parameters as seen in Fig. 11. The Reynolds and Weber number ranges for other cold flow experiments (Refs. 12-14) are also at least an order of magnitude lower than actual rocket conditions. The drop size comparisons between the cold flow and hot-fire conditions showed that the drops were larger for combusting conditions, suggesting that the gas phase velocity field between the two flowfields is significantly different.

ACKNOWLEDGEMENT

Funding by NASA Marshall Space Flight Center, Contract NAS 8-38862 and the Penn State NASA Propulsion Engineering Research Center, Contract NAGW 1356 Supplement 5, is acknowledged. The authors thank Mr. L. Schaaf for his assistance in conducting the experiments, Mr. W. E. Anderson and Mr. D. Harrje for their contributions to the design of the uni-element rocket chamber, and Mr. S. A. Rahman for his comments.

NOMENCLATURE

English Symbols

d inner diameter of LOX post

D drop diameter

F fuel (gaseous hydrogen)

\dot{m} mass flowrate

O oxidizer (liquid oxygen)

R radial distance

Re Reynolds number ($=\rho_l U d / \mu_l$) based on liquid properties, liquid jet velocity and post diameter

U velocity

We Weber number ($=\rho_l (U_g - U_l)^2 d / \sigma$) based on liquid properties, relative velocity and post diameter

Z axial distance

Greek Symbols

μ dynamic viscosity

ρ density

σ surface tension

Subscripts

D drop

g gas

l liquid

10 arithmetic mean

32 Sauter mean

REFERENCES

1. *Liquid Rocket Engine Injectors*, NASA SP-8089, 1976.
2. Hulka, J., Schneider, J. A. and Dexter, C. E., "Performance and Stability of a Booster Class LOX/H₂ Swirl Coaxial Element Injector," AIAA-91-1877, AIAA/SAE/ASME 27th Joint Propulsion Conference, Sacramento, CA, June 24-26, 1991.
3. Sutton, R. D., Schuman, M. D. and Chadwick, W. D., "Operating Manual for Coaxial Injection Combustion Model," NASA CR-129031, 1974.
4. Schuman, M. D. and Beshore, D.G., "Standardized Distributed Energy Release (SDER) Computer Program Final Report," AFRPL-TR-78-7, 1978.
5. Muss, J. A., Nguyen, T. V., and Johnson, C. W., "User's Manual for Rocket Combustor Interactive Design (ROCCID) and Analysis Computer Program," Volume 1 - User's Manual, NASA Contractor Report 1087109, May, 1991.
6. George, D. J., "Rocket Injector Hot Firing and Cold Flow Spray Fields," AIAA/SAE 9th Propulsion Conference, Las Vegas, NV., November 5-7, 1973.
7. George, D. J., "Droplet Size Distribution Functions for Rocket Combustor Spray Field," 11th JANNAF Combustion Meeting, Pasadena, CA., September 9-13, 1974.
8. Bachalo, W. D. and Houser, M. J., "Phase/Doppler Spray Analyzer for Simultaneous Measurements of Drop Size and Velocity Distribution," *Optical Engineering*, 23, 1984, pp. 583-590.

9. Ibrahim, K. M., Werthimer, G. D. and Bachalo, W. D., "Signal Processing Considerations for Laser Doppler and Phase Doppler Applications," The Fifth International Symposium on the Application of Laser Techniques of Fluid Mechanics, Lisbon, Portugal, July, 9-12, 1990.
10. *Liquid Particle Size Measurement Techniques, 2nd volume*, Hirleman, E. D., Bachalo, W. D., Felton, P. G. (eds.), ASTM, Philadelphia, 1990.
11. Vassallo, P., Ashgriz, N., and Boorady, F. A., "Effect of Flow Rate on the Spray Characteristics of Impinging Water Jets," *Journal of Propulsion and Power*, Vol. 8, No. 5, Sept-Oct. 1992, pp. 980-986.
12. Zaller, M. M. and Klem, M. D., "Coaxial Injector Spray Characterization Using Water/Air as Simulants," NASA-TM-105322, November, 1991.
13. Eroglu, H. and Chigier, N. A., "Initial Drop Size and Velocity Distributions for Airblast Coaxial Atomisers," *Journal of Fluids Engineering*, 113, 1991, pp. 453-459.
14. Hardalupas, Y., McDonald, H. and Whitelaw, J. H., "Two Fluid Mixing," *Advanced Earth-to-Orbit Propulsion Technology*, NASA Conference Publication 3174, Vol. II, 1992.
15. Goix, P. J., Cessou, A., Stepwoski, D. and Edwards, C. F., "Structure of a Methanol/Air Coaxial Reacting Spray near the Stabilization Region by OH Fluorescence Imaging and Two-Component Phase-Doppler Interferometry," 1992 Spring Meeting of the Western States Section, The Combustion Institute, Oregon State University, March, 1992.

16. Ryan, H. M., Pal, S., Lee, W., and Santoro, R. J., "Drop Distribution Effects on Planer Laser Imaging of Sprays," *Atomization and Sprays*, Vol. 2, No. 2, 1992, pp. 155-177.
17. Weast, R. C. (ed.), *Handbook of Chemistry and Physics*, 67th edition, p. E368, 1986.

Table 1: Property Comparisons

| | LOX | WATER | GH ₂ (@STP) | GN ₂ (@STP) |
|---|------|-------|---------------------------|---------------------------|
| ρ (kg/m ³) | 899 | 998 | 0.085 | 1.25 |
| μ (x10 ⁻⁵ kg/m s) | 8.25 | 98.8 | 0.872 | 1.73 |
| σ (x10 ⁻³ kg/s ²) | 4.8 | 73 | - | - |

Table 2: Flowrate Comparisons

| | HOT - FIRE | COLD FLOW | | |
|--------------------|------------|-----------|-------|-------|
| | | 1 | 2 | 3 |
| \dot{m}_l (kg/s) | 0.112 | 0.026 | 0.13 | 0.26 |
| U_l (m/s) | 13.5 | 2.9 | 14.3 | 28.0 |
| \dot{m}_g (kg/s) | 0.021 | 0.009 | 0.009 | 0.009 |
| U_g (m/s) | 381 | 293 | 293 | 293 |

Table 3: PDPA Results

| Run | R (mm) | D_{10} (μm) | D_{32} (μm) | U_D (m/s) | No. of Drops | % Val. | Run Time (sec.) |
|-----|-------------|-------------------------------|-------------------------------|----------------|-----------------|--------|-----------------------|
| 1 | 0.00 | 33.0 | 84.2 | 17.2 | 3756 | 42% | 4.00 |
| | | 53.2 | 114.9 | 17.6 | 149 | 16% | 1.41 |
| 2 | 3.18 | 33.6 | 86.3 | 17.0 | 3791 | 39% | 4.00 |
| | | 45.1 | 109.7 | 17.9 | 484 | 21% | 1.03 |
| 3 | 6.35 | 29.8 | 68.1 | 15.5 | 1136 | 56% | 4.00 |
| | | 28.2 | 71.0 | 17.2 | 448 | 46% | 1.52 |
| 4 | 9.53 | 27.7 | 97.8 | 16.7 | 115 | 53% | 4.00 |
| | | 26.8 | 57.5 | 12.9 | 45 | 62% | 0.82 |

Table 4: Rocket Chamber Conditions and Flowrates

| Run | Chamber Pressure (MPa)/ (psia) | LOX Flowrate \dot{m}_l (kg/s) | GH ₂ Flowrate \dot{m}_g (kg/s) | Mixture Ratio \dot{m}_l/\dot{m}_g (O/F) | Momentum Ratio \dot{m}_g/\dot{m}_l (F/O) | Velocity Ratio (F/O) | Re ($\times 10^5$) | We ($\times 10^5$) |
|-----|---|--|--|--|---|----------------------------|---------------------------|---------------------------|
| 1 | 2.79/404 | 0.120 | 0.021 | 5.6 | 4.70 | 26.8 | 4.97 | 1.61 |
| 2 | 2.72/395 | 0.110 | 0.021 | 5.2 | 5.58 | 29.2 | 5.11 | 1.95 |
| 3 | 2.73/396 | 0.113 | 0.021 | 5.3 | 5.19 | 27.9 | 5.25 | 2.07 |
| 4 | 2.43/352 | 0.103 | 0.019 | 5.5 | 5.41 | 29.3 | 4.80 | 2.59 |

Table 5: Hot-Fire/Cold Flow Comparisons

| | HOT - FIRE | COLD FLOW (CASE 2) | RATIO (H.F./C.F.) |
|-------------------------------|--------------------|-----------------------|----------------------|
| P_c (MPa)/ | 2.67 | 0.1 | 26.3 |
| (psi) | 387 | 14.7 | |
| ρ_l (kg/m ³) | 899 | 998 | 0.90 |
| ρ_g (kg/m ³) | 2.24 | 1.25 | 1.79 |
| \dot{m}_l (kg/s) | 0.112 | 0.13 | 0.85 |
| \dot{m}_g (kg/s) | 0.021 | 0.009 | 2.3 |
| \dot{m}_g/\dot{m}_l | 5.4 | 14.5 | 2.7 |
| U_l (m/s) | 13.5 | 14.3 | 0.94 |
| U_g (m/s) | 381 | 290 | 1.3 |
| U_g/U_l | 28.3 | 20.3 | 1.4 |
| $\dot{m}_g U_g/\dot{m}_l U_l$ | 5.3 | 1.4 | 3.8 |
| Re | 5.03×10^5 | 4.86×10^4 | 10.3 |
| We | 2.06×10^5 | 4.3×10^3 | 48 |

FIGURE CAPTIONS

Fig. 1. Cross-sectional view of the optically accessible rocket chamber. The chamber is modular in design and allows for change of the chamber length, injector assembly, window-section location and nozzle. The interior of the chamber is 50.8 x 50.8 mm. For the results presented here, the length of the chamber and nozzle throat diameter are 245.6 mm and 11.36 mm, respectively.

Fig. 2. Schematic of the shear coaxial injector.

Fig. 3. Phase Doppler Particle Analyzer (PDPA) setup for making drop size/velocity measurements in the uni-element rocket chamber. Both the transmitting and receiving optics are positioned 15° from the horizontal plane to yield a net 30° off-axis angle that is required for the measurements. The optics are mounted on translation stages thus allowing the probe volume to be traversed through the spray. Optical access through two sides of the rocket was afforded by 25.4 mm thick, 50.8 mm diameter quartz windows. In the rocket, the GH_2 and LOX flow into the page.

Fig. 4. The drop size number distributions measured by the PDPA for Run 2 (Table 3). The measured drop size number distribution for both the entire four second rocket firing and the 1.03 second steady pressure portion of the same firing are shown.

Fig. 5. Sauter mean diameter (D_{32}) versus nondimensional radial distance (R/d) for the water/ GN_2 shear coaxial injector sprays. The flowrate and velocity conditions are listed in Table 2.

Fig. 6. Mean drop velocity (U_D) versus nondimensional radial distance (R/d) for the water/ GN_2 shear coaxial injector sprays. The flowrate and velocity conditions are listed in Table 2.

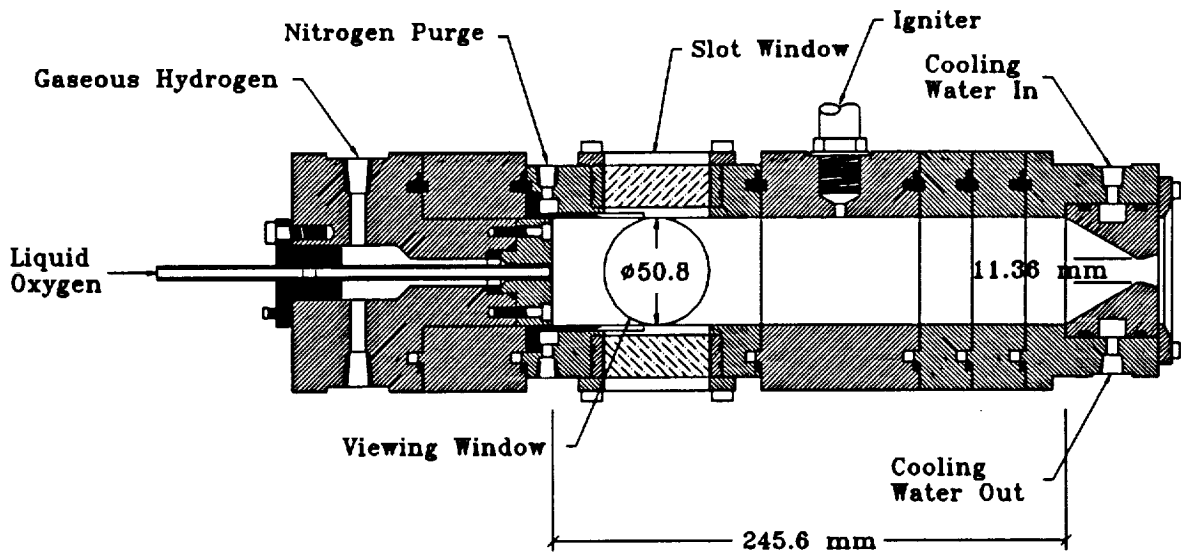
Fig. 7. Percent validation for PDPA drop size measurements versus nondimensional radial distance (R/d) in the water/ GN_2 shear coaxial injector sprays. The flowrate and velocity conditions are listed in Table 2.

Fig. 8. Number of samples per second for PDPA drop size measurements versus nondimensional radial distance (R/d) in the water/ GN_2 shear coaxial injector sprays. The flowrate and velocity conditions are listed in Table 2.

Fig. 9. Comparison of Sauter mean diameter (D_{32}) versus nondimensional radial distance (R/d) between hot-fire and cold flow conditions. The flow parameters for the two measurements are compared in Table 5.

Fig. 10. Comparison of mean drop velocity (U_D) versus nondimensional radial distance (R/d) between hot-fire and cold flow conditions. The flow parameters for the two measurements are compared in Table 5.

Fig. 11. Comparison of Reynolds versus Weber number ranges for the cold flow and hot-fire experiments with other cold flow experiments (Refs. 12-14) and examples of actual rockets.



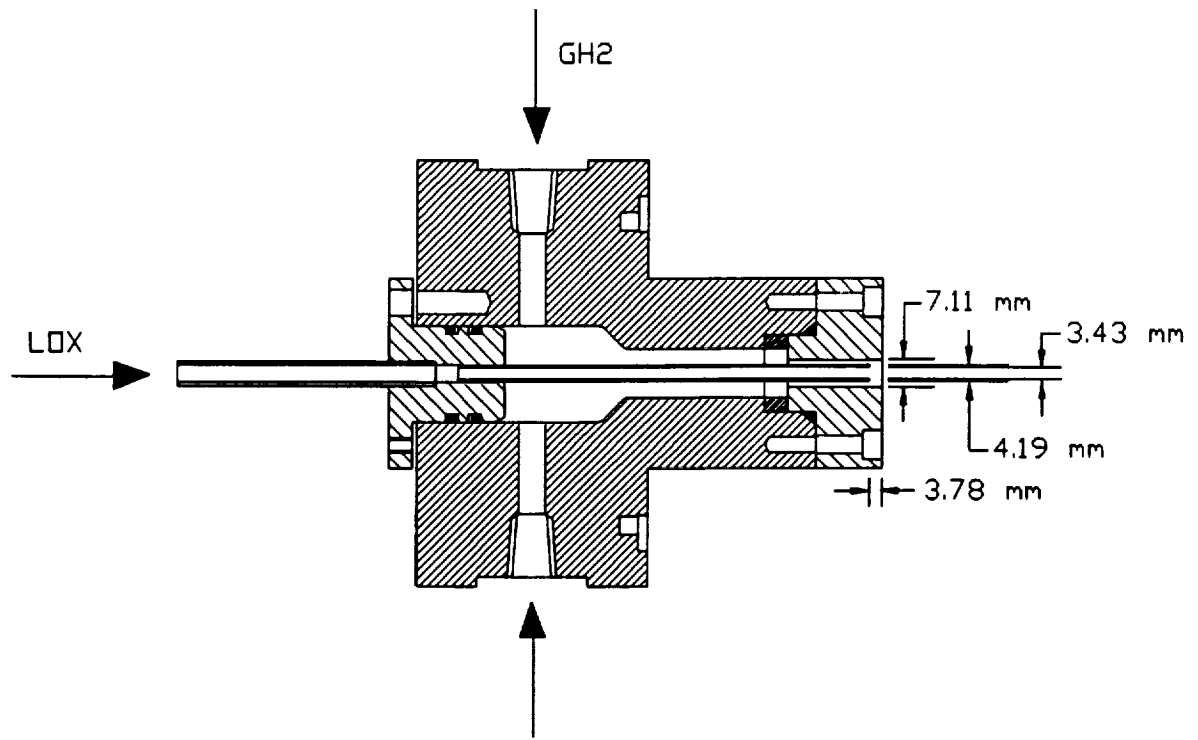


Fig 2

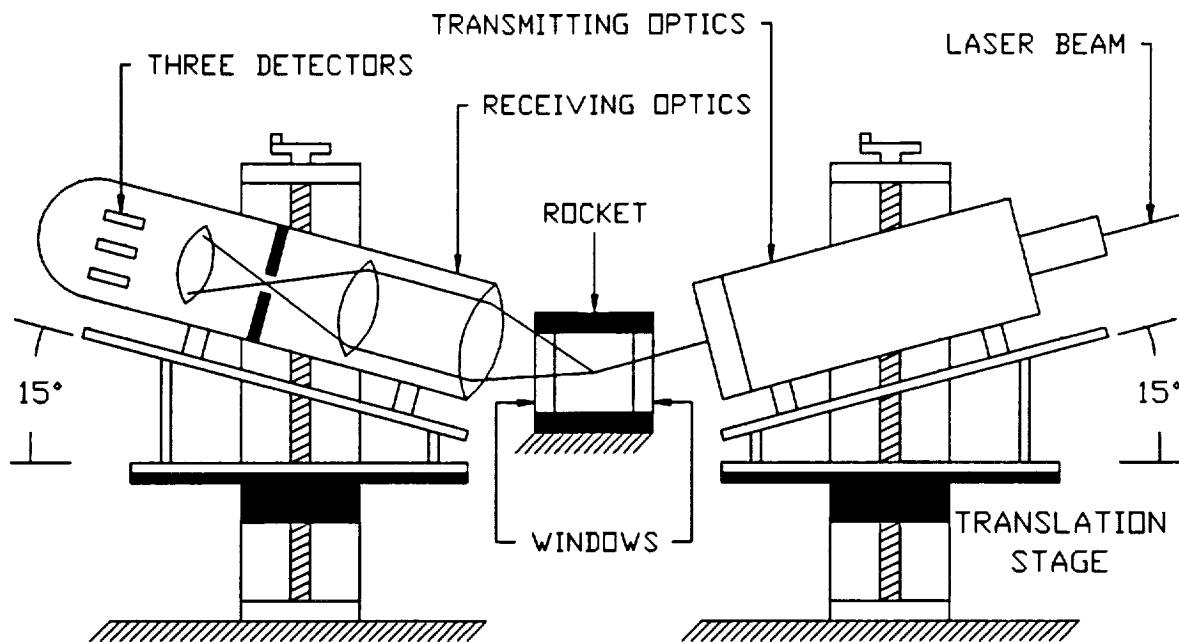
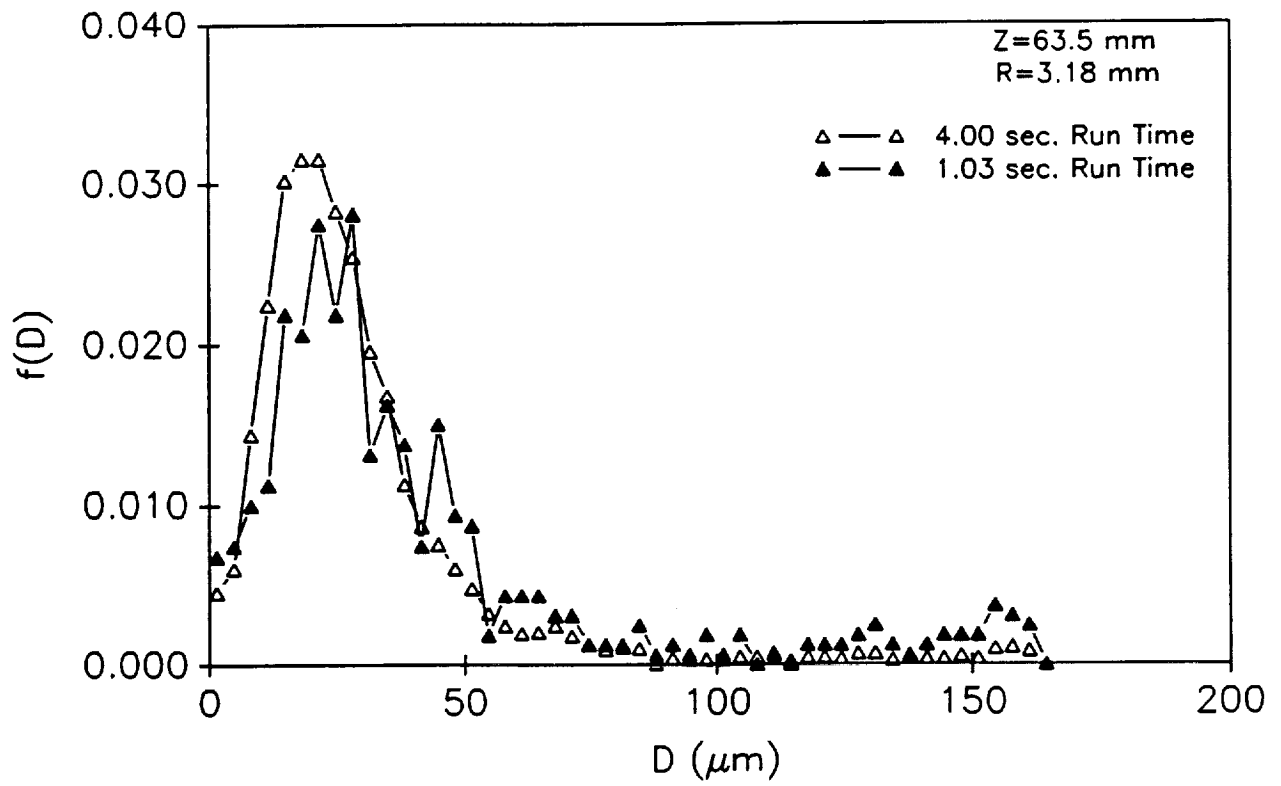


Fig. 3



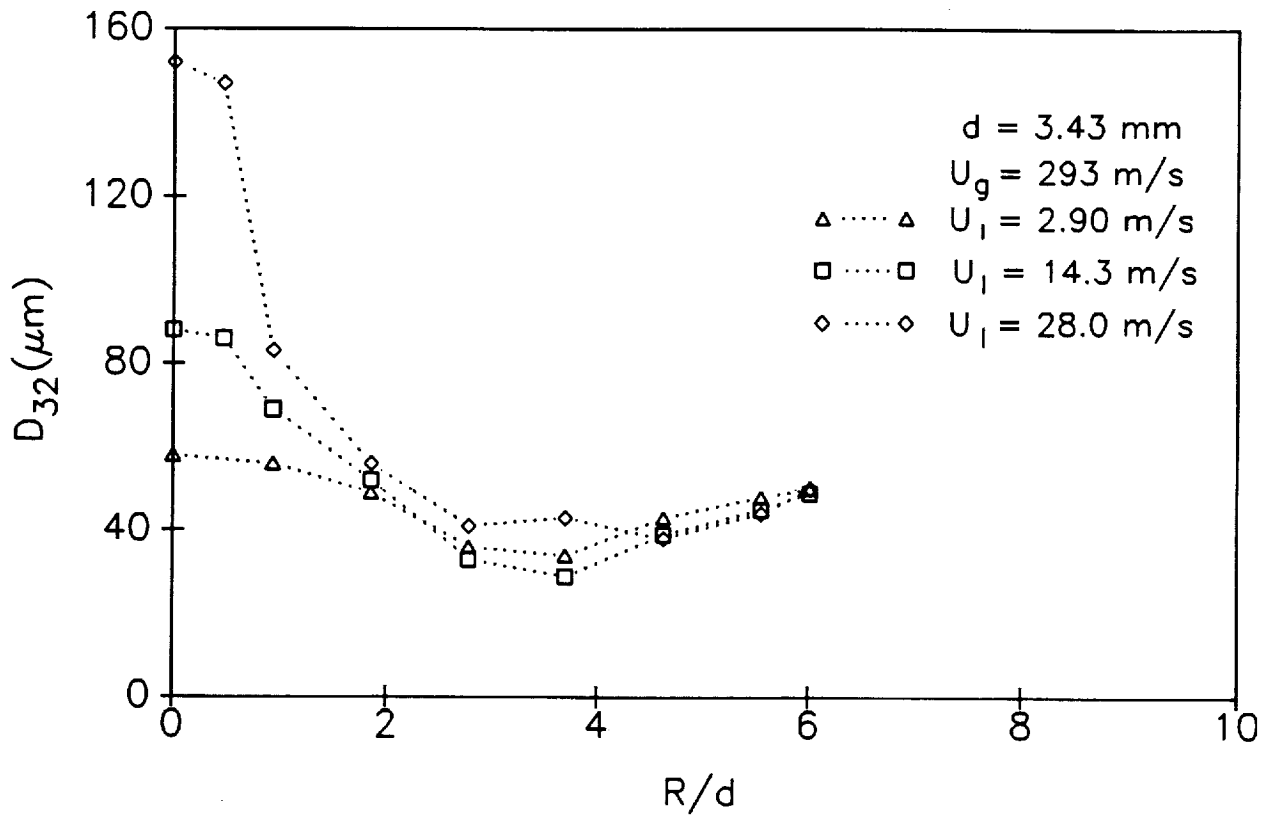


Fig. 5

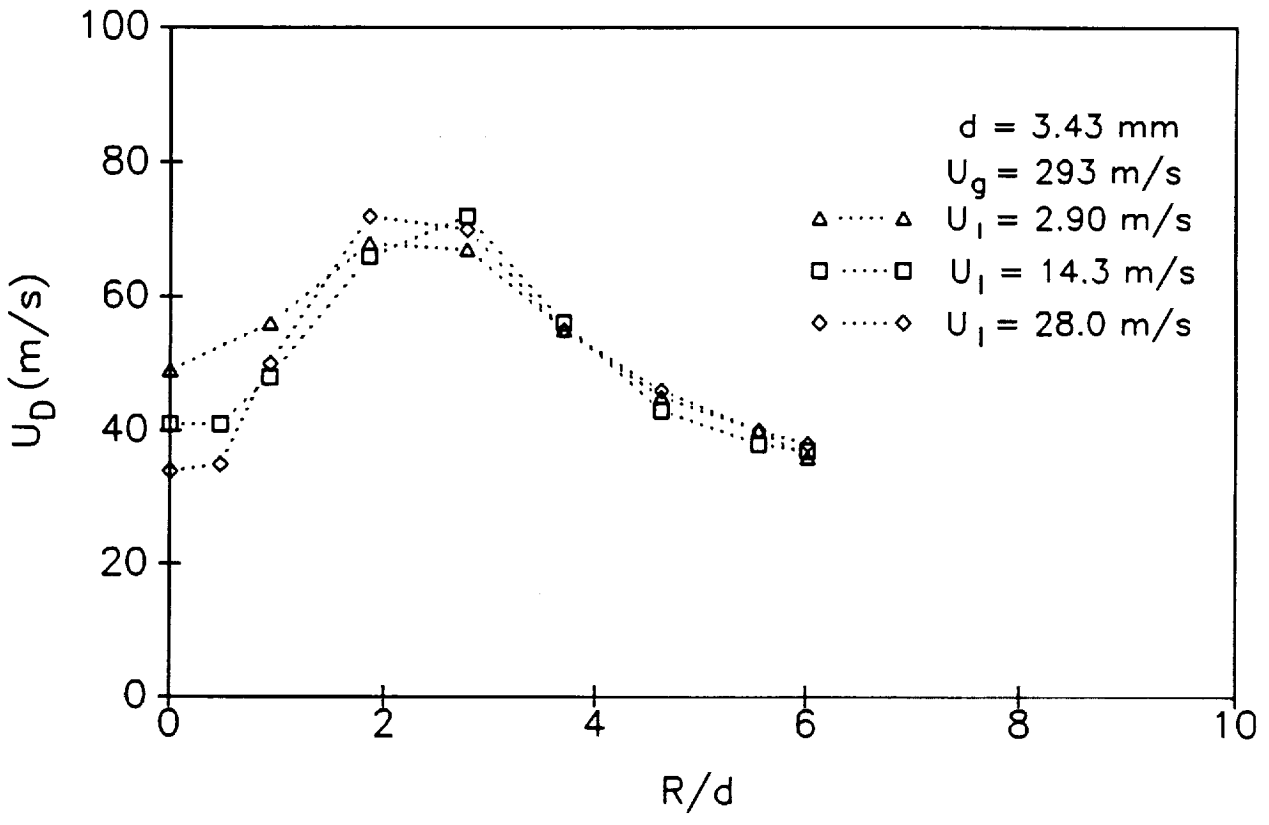
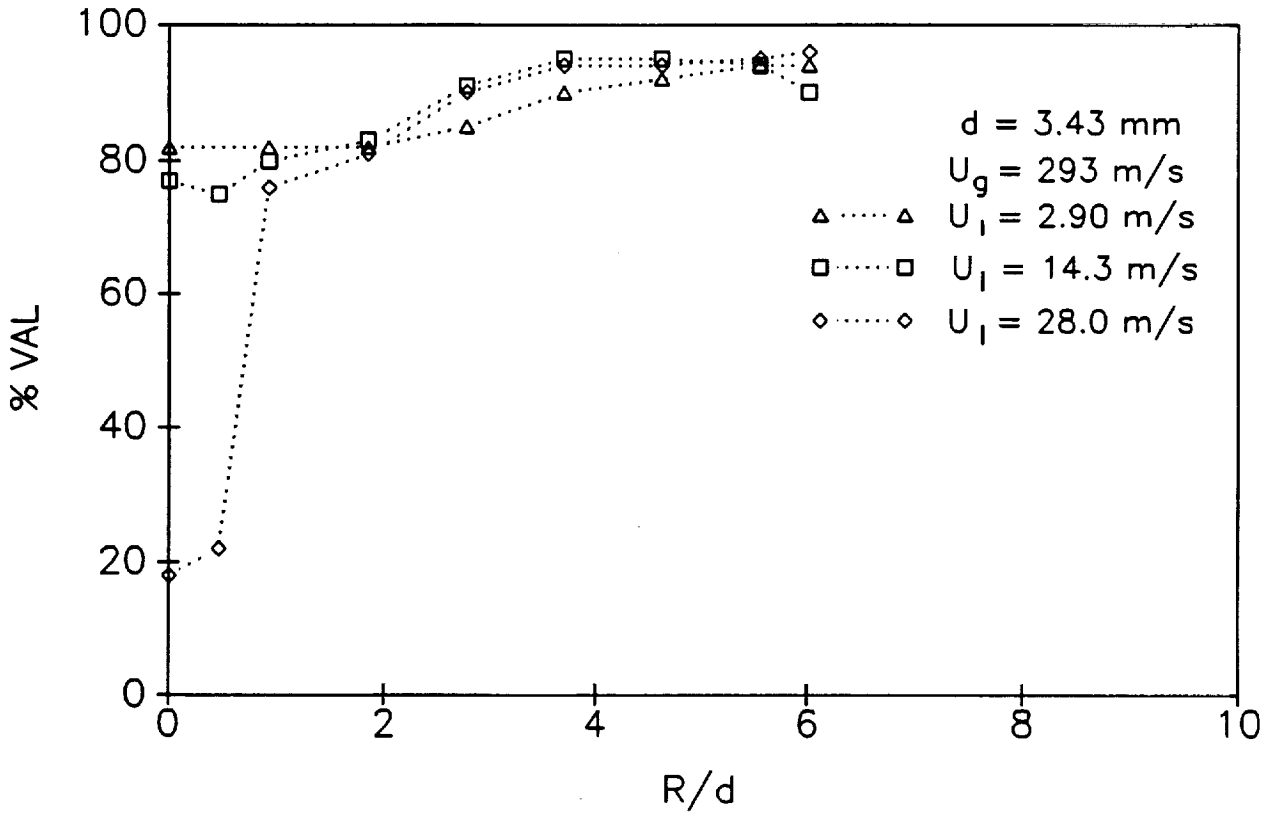


Fig. 6



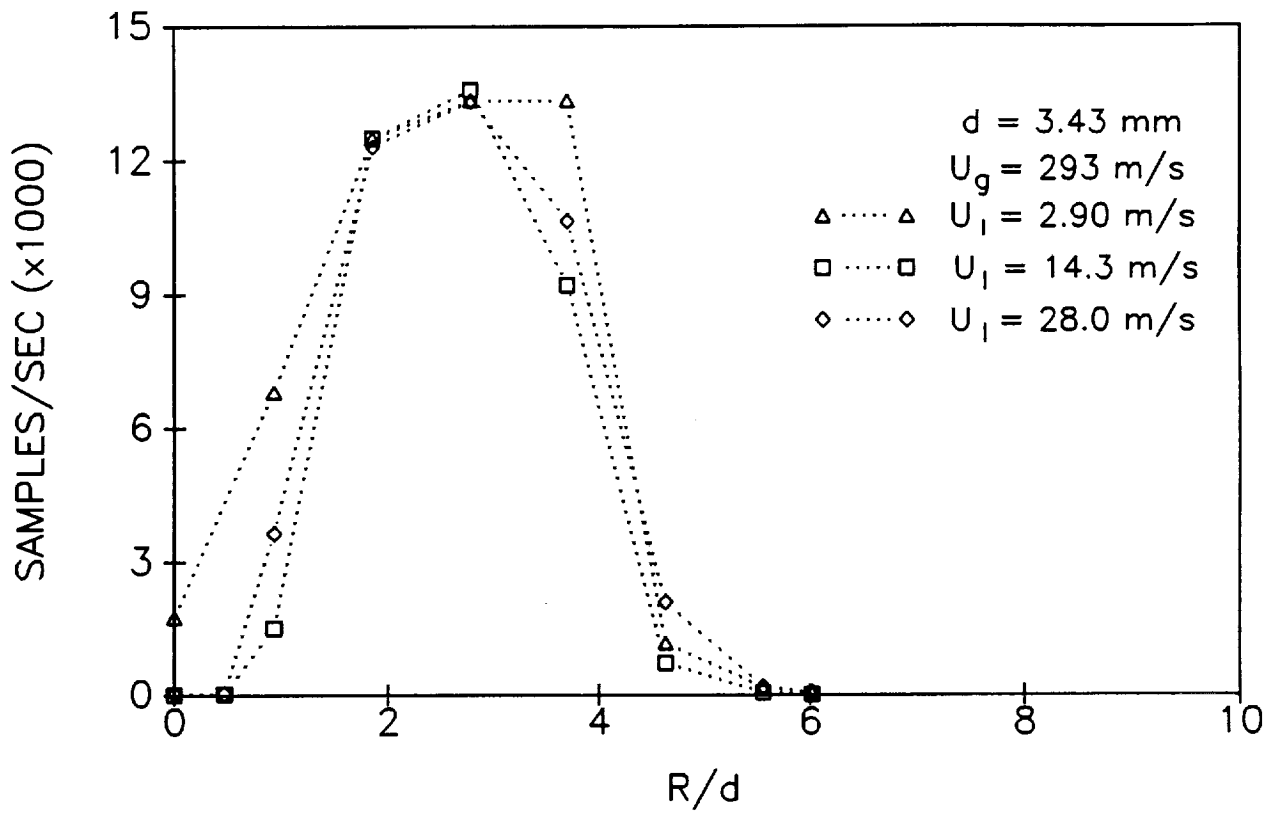


Fig. 8

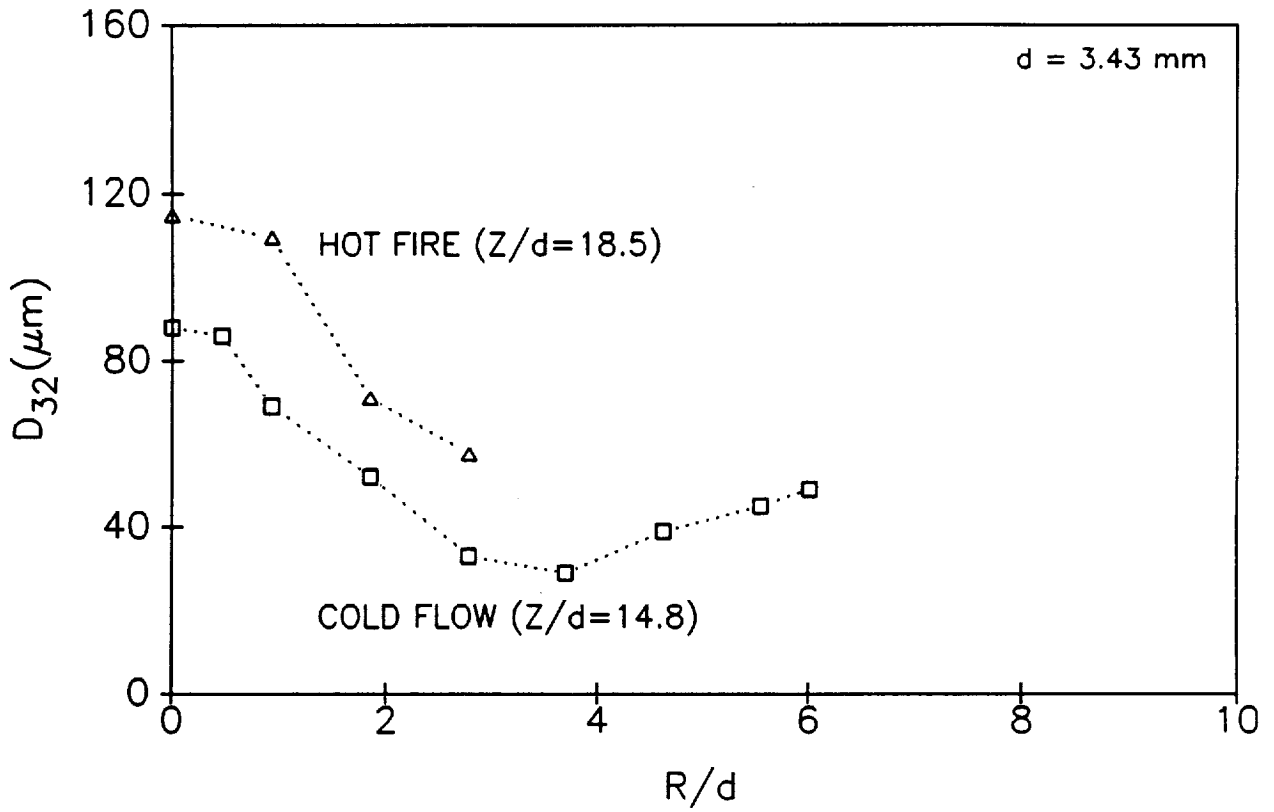


Fig. 9

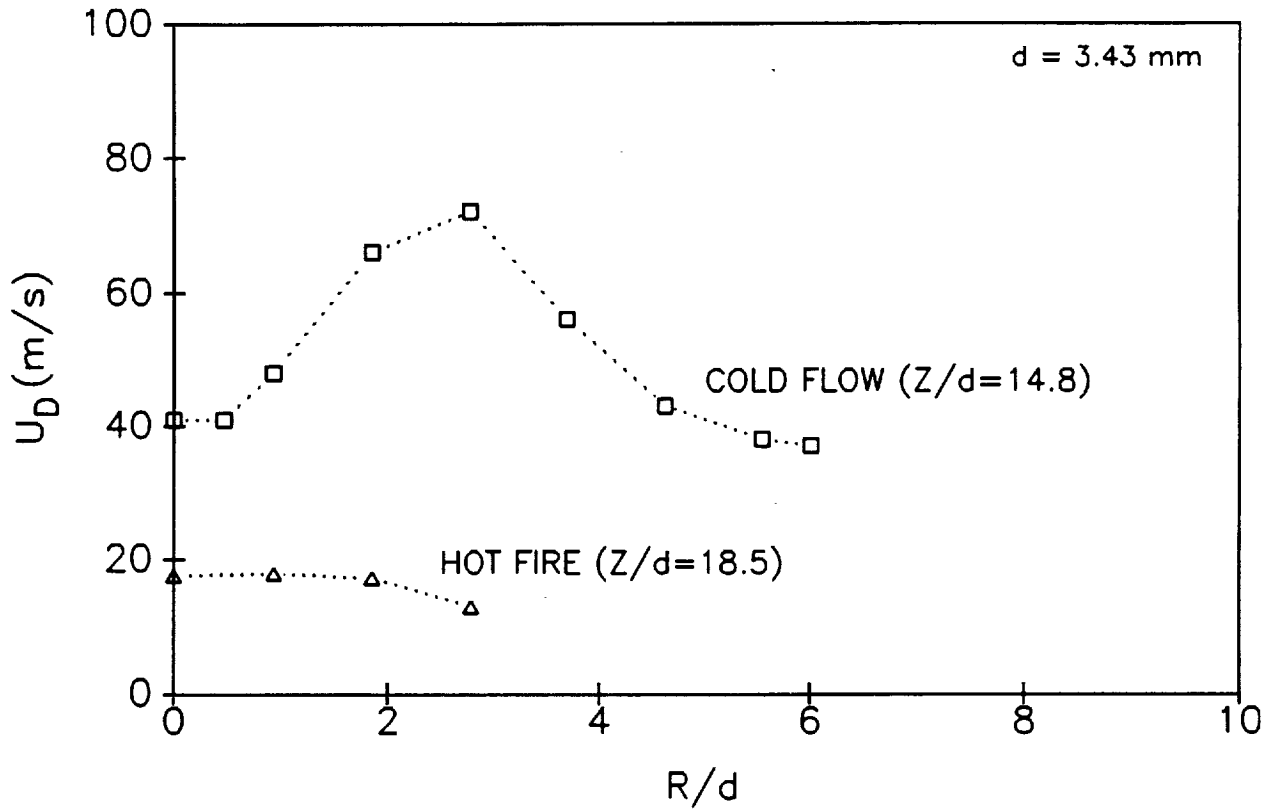


Fig. 10

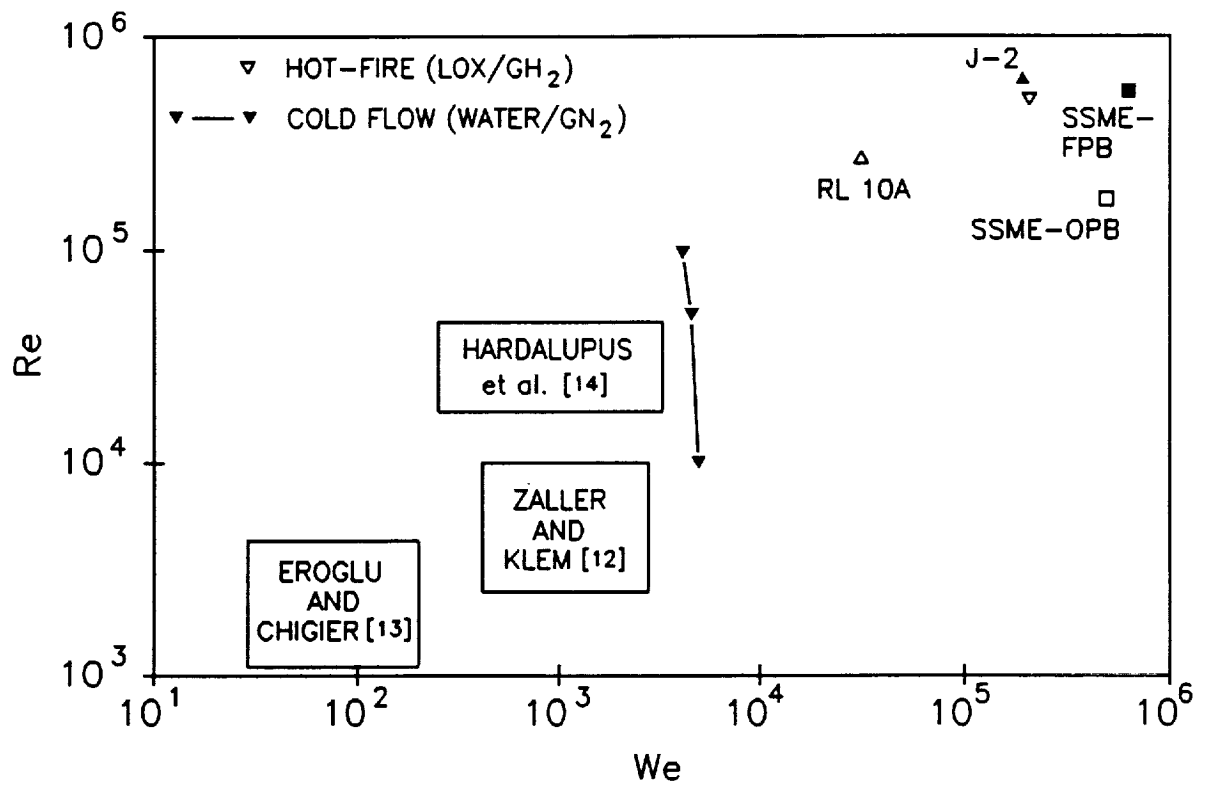


Fig. 11